

Pressure-actuated microfluidic devices for electrophoretic separation of pre-term birth biomarkers

V. Sahore¹ · S. Kumar¹ · C. I. Rogers¹ · J. K. Jensen¹ · M. Sonker¹ · A. T. Woolley¹

Received: 14 August 2015 / Revised: 7 October 2015 / Accepted: 21 October 2015 / Published online: 4 November 2015
© Springer-Verlag Berlin Heidelberg 2015

Abstract We have developed microfluidic devices with pressure-driven injection for electrophoretic analysis of amino acids, peptides, and proteins. The novelty of our approach lies in the use of an externally actuated on-chip peristaltic pump and closely spaced pneumatic valves that allow well-defined, small-volume sample plugs to be injected and separated by microchip electrophoresis. We fabricated three-layer poly(dimethylsiloxane) (PDMS) microfluidic devices. The fluidic layer had injection and separation channels, and the control layer had an externally actuated on-chip peristaltic pump and four pneumatic valves around the T-intersection to carry out sample injection. An unpatterned PDMS membrane layer was sandwiched between the fluidic and control layers as the actuated component in pumps and valves. Devices with the same peristaltic pump design but different valve spacings (100, 200, 300, and 400 μm) from the injection intersection were fabricated using soft lithographic techniques. Devices were characterized through fluorescent imaging of captured

plugs of a fluorescein-labeled amino acid mixture and through microchip electrophoresis separations. A suitable combination of peak height, separation efficiency, and analysis time was obtained with a peristaltic pump actuation rate of 50 ms, an injection time of 30 s, and a 200- μm valve spacing. We demonstrated the injection of samples in different solutions and were able to achieve a 2.4-fold improvement in peak height and a 2.8-fold increase in separation efficiency through sample stacking. A comparison of pressure-driven injection and electrokinetic injection with the same injection time and separation voltage showed a 3.9-fold increase in peak height in pressure-based injection with comparable separation efficiency. Finally, the microchip systems were used to separate biomarkers implicated in pre-term birth. Although these devices have initially been demonstrated as a stand-alone microfluidic separation tool, they have strong potential to be integrated within more complex systems.

Keywords Microfluidics/microfabrication · Capillary electrophoresis/electrophoresis · Bioanalytical methods

✉ A. T. Woolley
atw@byu.edu

V. Sahore
sahore@byu.edu

S. Kumar
kumarsuresh444@gmail.com

C. I. Rogers
chadirogers@gmail.com

J. K. Jensen
jkj728@gmail.com

M. Sonker
mukul.sonker89@gmail.com

¹ Department of Chemistry and Biochemistry, Brigham Young University, Provo, UT, USA

Introduction

Micro total analysis systems (μTAS) are of interest for chemical and biological studies and hold the promise of portable, rapid, sensitive, and inexpensive point-of-care analysis [1–3]. To realize this goal, integration of multiple processes, such as chemical reactions, analyte capture, extraction, and labeling, and sample mixing, transport, separation, and detection on a miniaturized platform, is important [3–5]. Many studies have been performed in this direction, including on-chip sample pre-concentration and labeling for protein analysis [6], integration of microchip electrophoresis with immunoaffinity extraction for multiple biomarker detection in human serum [7],

development of an integrated platform for the extraction and quantification of ovarian cancer cells from whole blood [8], construction of a simple platform for pesticide detection [9], and a chip-based integrated system for DNA sample preparation and amplification to detect pathogens in food samples [10].

Microchip electrophoresis (μ CE) is a powerful component of many miniaturized analysis systems [3, 11–13]. Standard μ CE device operation requires the analyte to be loaded into the injection intersection, which can be done by applying either voltage or pressure across the injection channel [14]. Most studies have used electrokinetic injection for reasons such as device fabrication ease, automated and simple operation, and established theoretical models [11, 15–17]. However, electrokinetic injection also has several downsides: it is ineffective with either low- or high-conductivity samples, analyte loading is biased by electrophoretic mobilities for short injection times (tens of seconds, depending on device layout and analytes), and it becomes increasingly difficult to implement effectively as integrated designs become more complex [11, 14, 18].

One potential solution to these challenges with electrokinetic injection is to use pressure-driven injection. Hydrodynamic injection has been used in the separation of model neurotransmitters [19] and studies of hydrophobic ligand binding [20]; however, the sample was injected using off-chip pressure, and the microfluidic devices lacked the on-chip controls needed to automate sample movement. An on-chip pump and valve architecture can provide small-volume control, improving analysis. In some applications, microfluidic devices were manufactured with pneumatic valves to guide sample movement, but pressure was applied through an external syringe pump, which generated large dead volumes [21–25]. Bowen et al. [26] advanced this concept further by developing a microfluidic device with an externally actuated on-chip peristaltic pump and pneumatic valves to perform μ CE with electrochemical detection of neurotransmitters. Although that work provided a strong foundation for externally actuated on-chip pressure-based control of injection for μ CE, the sample plug size was affected by the injection time, and longer injection times increased sample diffusion into the separation channel. Furthermore, although the reversible sealing between poly(dimethylsiloxane) (PDMS) and glass allowed multiple uses and cleaning between assays, the robustness of the PDMS glass bond was a limitation. Herein, we demonstrate a three-layer PDMS microfluidic device that pumps sample to the injector and captures a defined sample plug using four externally actuated pneumatic valves surrounding the intersection. These devices operate with fast pump actuation times (<50 ms) and provide consistent results with long (~2 min) injection times, generating precise, discrete, and reproducible sample plugs.

Pre-term birth (PTB) is the most common complication of pregnancy and is considered to be the primary cause of newborn deaths and illnesses [27–29]. PTB risk can be predicted weeks before contractions occur through the detection of specific molecular markers in bodily fluids [30]; recently, a serum biomarker panel of three peptides and six proteins was demonstrated to provide specific (~80 %) and sensitive (~90 %) prediction of a pre-term delivery occurring four or more weeks later [31–33]. In this work, we optimized the fabrication of multi-layer PDMS microfluidic devices for PTB biomarker analysis. The fluidic layer had injection and separation channels, and the control layer had a peristaltic pump and four pneumatic valves around the T-intersection to carry out sample injection and plug capture. An unpatterned PDMS membrane was sandwiched between the fluidic and control layers as the actuated component in the pump and valves. Microchips with the same peristaltic pump design but different valve spacings (100, 200, 300, and 400 μ m) from the T-intersection were manufactured. Devices were characterized by fluorescent imaging of a captured plug of a fluorescein-labeled amino acid mixture and through μ CE separations. We found that a pump actuation rate of 50 ms, a 30-s injection time, and a 200- μ m valve spacing provided a suitable combination of peak height, separation efficiency, and speed of analysis. We demonstrated the ability to inject samples prepared in different solutions and achieved a 2.4-fold improvement in signal and 2.8-fold increase in separation efficiency through field-amplified stacking. A comparison between pressure-driven and electrokinetic injection with the same injection time and separation voltage showed a 3.9-fold increase in peak height with pressure-driven injection. Finally, we used these devices to separate two model biomarkers that are implicated in pre-term birth. These studies form a strong foundation for subsequent development of a more highly integrated microfluidic system for PTB biomarker determination.

Experimental section

Chemicals and materials

Hydroxypropyl cellulose (HPC), arginine, phenylalanine-alanine (FA), phenylalanine-glycine-glycine-phenylalanine (FGGF), glycine-glycine-tyrosine-arginine (GGYR), and dimethyl sulfoxide (DMSO) were purchased from Sigma-Aldrich (St. Louis, MO). Sodium bicarbonate and glycine were obtained from EMD Chemical (Gibbstown, NJ), and phenylalanine was purchased from Spectrum Chemical (Gardena, CA). Ferritin was purchased from EMD Millipore (Billerica, MA), and fluorescein-labeled peptide 1 was obtained from GenScript USA (Piscataway, NJ). PDMS base and curing agent used to make the devices were obtained from Dow Chemical (Midland, MI). AZ P4620 and SU-8 2025

photoresists, used for fluidic and control layer template fabrication, were purchased from EMD Millipore (Somerville, NJ) and MicroChem (Westborough, MA), respectively. Fluorescein isothiocyanate (FITC) used to label the analytes was purchased from Life Technologies (Carlsbad, CA). All solutions were made in deionized (DI) water filtered by a Barnstead Water Purifier (Thermo Scientific, Waltham, MA).

Microchip design

Microfluidic chips were designed using CleWin software (Informer Technologies, Shingle Springs, CA) with the layout shown in Fig. 1a. Each microfluidic chip had three layers of PDMS (Fig. 1b). The bottom was a fluidic layer with 100 μm wide injection and separation channels having sample (S), sample waste (SW), buffer (B), and buffer waste (BW) reservoirs. The distance between the S, SW, and B reservoirs and the T-intersection was 1 cm, whereas the distance from the BW reservoir to the T-intersection was 1.5 cm. The middle layer was a $\sim 30\text{-}\mu\text{m}$ -thick unpatterned membrane, actuated to manipulate fluid. The top control layer had a three-valve peristaltic pump and four pneumatic valves surrounding the intersection for plug capture. The width of all pneumatic valves was 150 μm , and the spacing between the peristaltic pump valves was 150 μm . Four different valve designs with 100, 200, 300, and 400 μm spacing from the T-intersection were used to capture the sample plug.

Device fabrication

Device layers were fabricated using soft lithography [26] and were thermally bonded. A 10-cm-diameter, 0.6-mm-thick bare silicon wafer (Silicon Desert, Tempe, AZ) was used to make the lithographic masters (Fig. 2a). To remove the native oxide, the silicon wafers were etched using buffer oxide etchant (Transene, Danvers, MA) for 30 s. Thermally dried wafers were exposed to hexamethyldisilazane (SPI Supplies, West Chester, PA) vapor for 5 min, followed by application of AZ P4620 or SU-8 2025 photoresist for fluidic or control layer master fabrication, respectively. Photoresist-coated wafers were exposed to UV light through design masks in a Karl Suss MA 150 mask aligner (Karl Suss America, Waterbury, VT) as shown in Fig. 2b. Wafers were then developed in AZ 400K (AZ Electronics, Somerville, NJ) or SU-8 (Microchem, Newton, MA) developer solution for fluidic or control layers, respectively (Fig. 2c). After a post-development bake at 150 $^{\circ}\text{C}$ for 5 min, the silicon masters were ready for PDMS pattern transfer, and each silicon master had four device designs on it.

Before PDMS processing, the masters were silanized using tridecafluoro-1,1,2,2-tetrahydrooctyl-1-trichlorosilane vapor (Gelest, Morrisville, PA) at 80 $^{\circ}\text{C}$ for 10 min. A mixture of PDMS base and curing agent (4:1) was poured on the silanized fluidic and control masters and thermally cured at

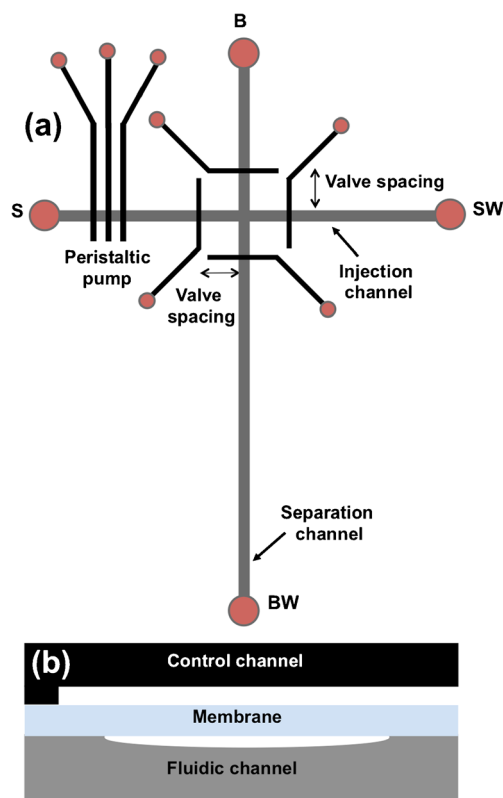


Fig. 1 Device schematic. **(a)** Top-down view of the microchip design, showing peristaltic pump and pneumatic valves around the T-intersection. Four different valve spacings were used. *S* sample, *SW* sample waste, *B* buffer, *BW* buffer waste. **(b)** Cross-sectional view of an unpatterned membrane sandwiched between the control and fluidic channel layers

80 $^{\circ}\text{C}$ for 1 h (Fig. 2d). For the unpatterned PDMS membrane layer, a mixture of PDMS base and curing agent (20:1) was spun (2,500 rpm, 1 min) on a silanized silicon wafer followed by baking at 80 $^{\circ}\text{C}$ for 1 h. Thermally cured control and fluidic PDMS layers were peeled off, and individual devices were cut out (Fig. 2e). The depth of control and fluidic layer channels was ~ 28 and ~ 20 μm , respectively. For the control layer, injection holes were punched using a 22-gauge blunt end needle (Jenson Global, Santa Barbara, CA) that allowed the solenoid tubes to be inserted inside. After hole punching, the control layer was stamp-coated with a thin film of PDMS curing agent and thermally bonded to the unpatterned PDMS membrane at 80 $^{\circ}\text{C}$ for 1 h (Fig. 2f). The bonded control/membrane assembly was aligned under an in-house built optical inspection microscope with the fluidic layer also stamp-coated with a thin film of PDMS curing agent and thermally bonded at 80 $^{\circ}\text{C}$ for 1 h (Fig. 2g). At this stage, reservoir holes were punched in the three-layer structure device using a 2.5-mm-diameter biopsy needle (Miltex, York, PA). For operational convenience, 20:1 PDMS was coated and thermally cured on a glass slide at 80 $^{\circ}\text{C}$ for 1 h. The three-layer device was then bonded to this PDMS-coated glass slide at 80 $^{\circ}\text{C}$ for 1 h (Fig. 2h) and was ready for electrophoretic separation and fluorescence detection experiments.

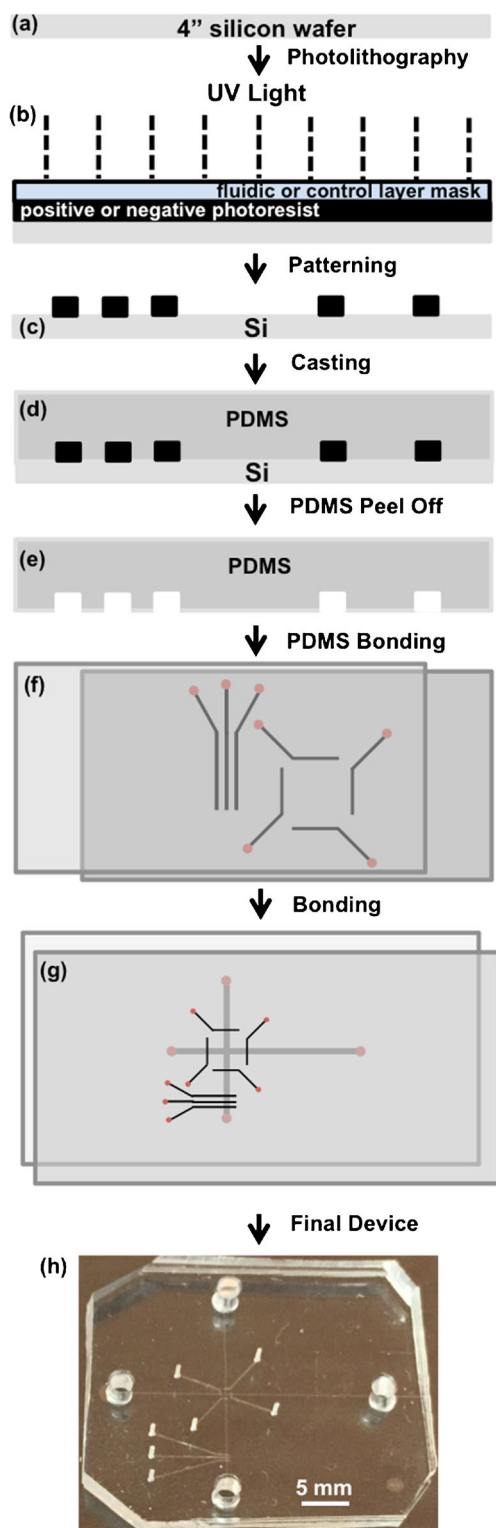


Fig. 2 Microfluidic device fabrication procedure. (a) A silicon wafer is used as the substrate for soft lithography. (b) The layer mask design is transferred to the silicon wafer using photoresist, followed by (c) photoresist development. (d) A mixture of PDMS base and curing agent is deposited and thermally cured on the silicon wafer. (e) The design from the patterned silicon wafer is transferred to the cured PDMS, which is peeled off. (f) An unpatterned PDMS membrane is thermally bonded to the control layer, followed by (g) bonding to the fluidic channel layer. The three-layer structure is thermally bonded to a PDMS-coated glass slide to make the final device. (h) Device photograph

electrodes connected to a power supply (Stanford Research Systems, Sunnyvale, CA). Laser-induced fluorescence detection was performed in a system with 488 nm laser excitation (JDSU, Shenzhen, China), and a photomultiplier tube (PMT; Hamamatsu, Japan), for point detection or a charge-coupled device (CCD) camera (CoolSnap HQ; Photometrics, Tucson, AZ) for plug capture imaging [6, 15]. The on-chip pump and valves were actuated by external pressure applied through a ten valve solenoid manifold (Clippard Instrument, Cincinnati, OH) controlled with LabView software (National Instruments, Austin, TX) through a home-built electronic circuit. Plastic tubing was filled with the colored dye solution, and on-chip connections were made thereafter. A 30-psi actuation pressure was applied to close the pneumatic valves, and a separation voltage of +1,000 V was used for μ CE. Laser-induced fluorescence detection was done at a 1-cm distance from the T-intersection. All the data were analyzed using an algorithm developed in MATLAB software.

Device operation

All samples loaded in devices were prepared in 10 mM bicarbonate buffer (BCB, pH 10.1), unless stated otherwise. For labeling, analyte solutions were mixed 9:1 by volume with 10 mM FITC in DMSO and were allowed to react overnight. Before experimentation, every device was washed with 2-propanol, DI water, and 10 mM BCB, with vacuum drying between each step. Subsequently, the devices were filled with running buffer (20 mM BCB, 15 mM NaCl, 0.01 % HPC, pH 10) and allowed to sit for 5 min. For typical device operation, the separation channel valves were closed, while injection valves were left open, followed by peristaltic pump actuation (see Fig. 3a). After a set injection time, the peristaltic pump was shut off and the injection valves were closed, thus capturing the sample plug as shown in Fig. 3b. The inset photograph shows all four valves closed (400 μ m spacing). Immediately thereafter, the separation valves were opened followed by the application of the separation voltage (see Fig. 3c). Under the applied voltage, the sample plug moved down the channel and its fluorescence was probed at the detection point. For comparison, μ CE was also performed with a pinched sample injection [34, 35]

Experimental setup

A microfluidic device was secured on the stage of a Nikon Eclipse TE 300 microscope (Nikon, Melville, NY), and connections to solenoids were made using plastic tubing. Voltage was applied to the solution reservoirs using platinum

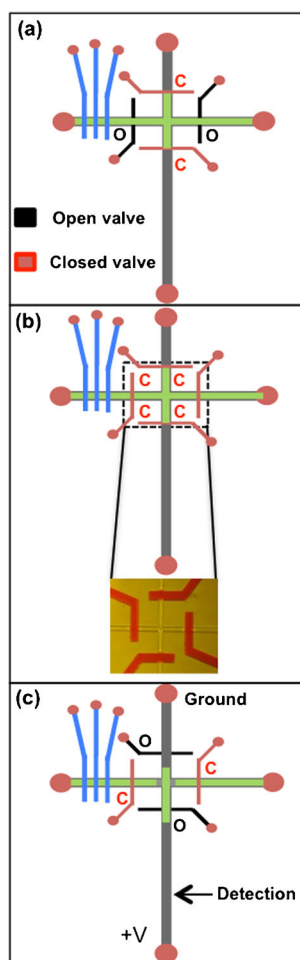


Fig. 3 Device operation. (a) Injection: with closed separation valves, the peristaltic pump (blue) loads sample through the injection channel. (b) Plug capture: after the set injection time, the injection valves are closed and the pump is shut off, thus allowing sample plug capture. A plug captured by closed valves that contain red dye solution (inset). (c) Separation: with injection valves closed and separation valves open, the captured plug is separated by μ CE and detected by laser-induced fluorescence

using a PDMS device with 200 μ m valve spacing but without actuating the peristaltic pump and valves. Here, the injection voltage was +500 V at SW with all other reservoirs grounded, and the separation voltage was +1,000 V at BW, with S and SW at +500 V and B grounded.

Results and discussion

Optimization of pump actuation rate and injection time

We studied the effects of pump actuation rate and sample injection time on separation performance in these devices. As seen in Fig. 4a, we separated FITC-labeled glycine and arginine by μ CE. Figure 4b shows the variation in peak height and number of theoretical plates for the glycine

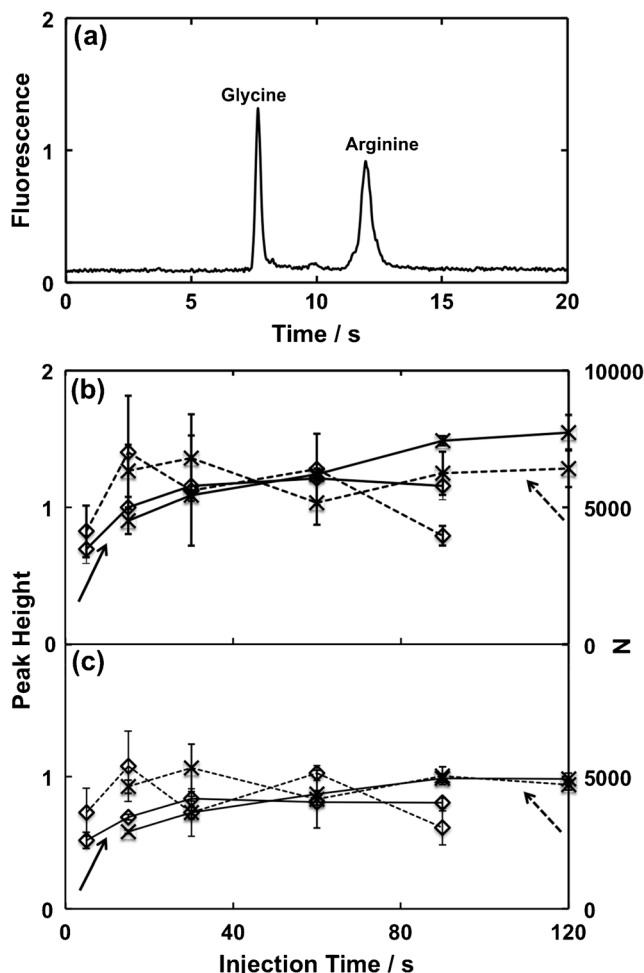


Fig. 4 Effects of pump actuation rate and injection time on separation. (a) Microchip electropherogram showing separation of FITC-labeled glycine and arginine (200 nM each), using a 50-ms pump actuation rate and 30 s injection time. (b, c) Peak height (solid line) and number of theoretical plates, N (broken lines), for (b) glycine and (c) arginine as a function of injection time for 50 (diamond) and 100 (cross) ms pump actuation rates. Error bars represent the standard deviation for five injections. Devices with a 200- μ m valve spacing were used for all experiments

peak. For the 50-ms actuation rate, the peak height increased going from 5 to 30 s injection time but then remained flat for longer injection times. For the 100-ms actuation rate, the peak height had a gradual, small increase going from 15 to 120 s injection times. The number of theoretical plate data showed a small variation of about the same magnitude as the standard deviation for both 50 and 100 ms actuation rates, with no clear trend as a function of injection time. Figure 4c shows the peak height and theoretical plate data for arginine; the same patterns as for glycine were observed. Considering the data, we chose a 50-ms actuation rate and 30-s injection time for future experiments because this provided a good combination of analysis speed, peak height, and number of theoretical plates.

Valve spacing optimization

Our devices offer the flexibility of capturing different volume plugs depending on the design, thus offering advantages for miniaturized separation. The selection of valve spacing was expected to affect both the peak height and separation efficiency. Valve spacing was optimized by separating a mixture of FITC-labeled FA, FGGF, and GGYR (each 300 nM). Baseline-resolved, vertically offset, microchip electropherograms for the separation of these peptides are shown as a function of valve spacing in Fig. 5a. The migration time of analytes varied somewhat with different valve spacings, possibly because of small differences in the distance from the injector to where detection was performed. Figure 5b shows the peak height as a function of valve spacing for the three peptides. The data show a maximum peak height for all the peptides at a 200- μm valve spacing, with slightly smaller heights for 100, 300, or 400 μm spacing. We note that the difference in peak heights is not large and that there is some scatter in the data as well. With the 100- μm valve spacing, the decrease in peak height relative to the 200- μm spacing is probably due to the smaller quantity of sample injected. The decrease in peak height for the 300- and 400- μm valve spacing is possibly due to plug dilution during injection because the loading process does not fully fill the space between the two separation valves. Fluorescent CCD images of a fluorescein-labeled glycine, phenylalanine, and arginine mixture (3 μM each) in Fig. 5d support this hypothesis: the fluorescent plug length is essentially the same for 200, 300, and 400 μm valve spacings. Figure 5c shows the number of theoretical plates as a function of valve spacing for the three peptides. The number of theoretical plates shows a much less pronounced variation with valve spacing, compared to peak heights. Indeed, the magnitude of the standard deviations of number of theoretical plates exceeds the differences for various valve spacings, indicating moderate reproducibility and that the number of theoretical plates has limited dependence on valve spacing in our experiments. The number of theoretical plates in μCE depends on several factors, including diffusion, injected plug length, and other dispersive factors [34]. Figure 5d shows that the injected plug lengths are essentially the same for 200–400 μm valve spacing, which may help explain why the number of theoretical plates is not affected significantly by valve spacing. Alternatively, if peak dispersion inherent to using PDMS as a device material is the main constraint for the number of theoretical plates, then the theoretical plate counts would likewise have limited dependence on valve spacing. Based on the improved peak height with 200 μm valve spacing, this design parameter was chosen for future studies.

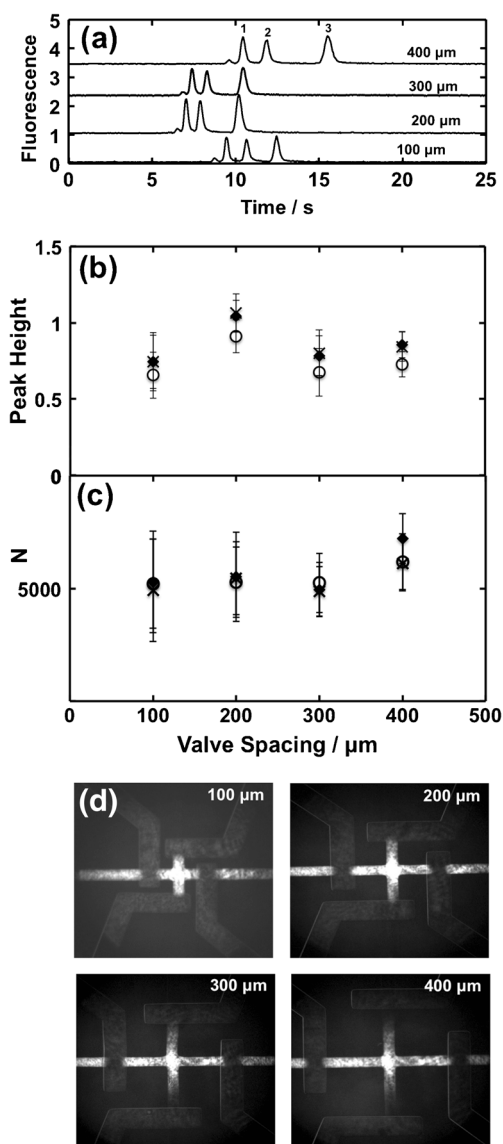


Fig. 5 Optimization of valve spacing. **(a)** Microchip electropherograms of peptides, 1 FA, 2 FGGF, and 3 GGYR, for different valve spacings. **(b)** Peak height and **(c)** number of theoretical plates (N), as a function of valve spacing. FA: black diamond, FGGF: white circle, GGYR: cross. Error bars represent the standard deviation for 16 injections, done using two different microfluidic devices. **(d)** CCD images (500 ms exposure time) of fluorescence from FITC-labeled glycine, phenylalanine, and arginine (3 μM each) captured in the injection intersection with different valve spacings. A 50-ms pump actuation rate and a 30-s injection time were used for all experiments

Effects of sample stacking

In the previous experiments, the sample solutions were made through serial dilution from 1 mM stock in 10 mM BCB, which had a different ionic strength from the running buffer (20 mM BCB, 15 mM NaCl, 0.01 % HPC, pH 9.8). Thus, we studied the effects of sample stacking. Figure 6a shows μCE of FITC-labeled glycine and arginine (200 nM each)

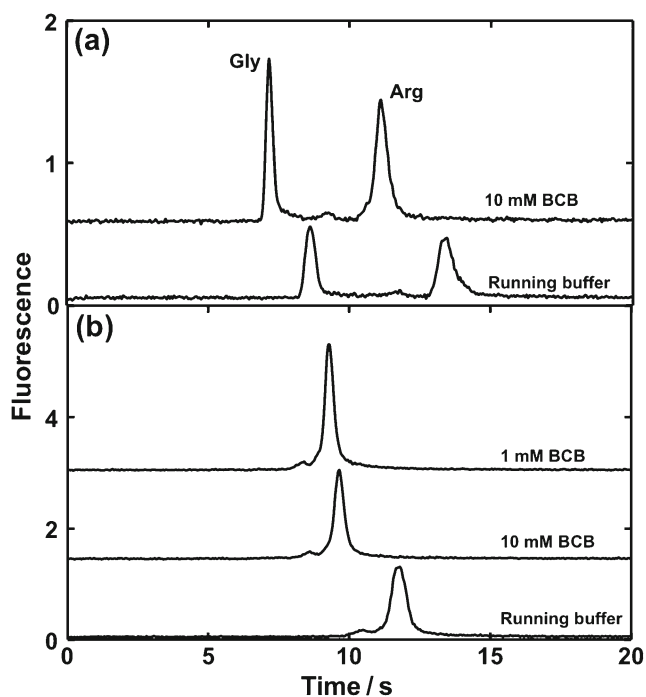


Fig. 6 Effects of sample stacking on μ CE. (a) Microchip electropherograms of separation of glycine and arginine (each 200 nM) in 10 mM BCB and running buffer. (b) Microchip electropherograms of FITC-labeled peptide 1 (1 μ g/mL) in running buffer, 10 mM BCB, and 1 mM BCB. A pump actuation rate of 50 ms, injection time of 30 s, and 200 μ m valve spacing were used for all experiments. The electropherograms are offset vertically

prepared in either 10 mM BCB or running buffer. A comparison of peak height shows increases of 2.4- and 2.1-fold for glycine and arginine, respectively, in 10 mM BCB where stacking occurs compared to running buffer. A comparison of the number of theoretical plates shows 2.8- and 1.6-fold increases for glycine and arginine, respectively, in 10 mM BCB compared to running buffer. A similar stacking experiment was performed with peptide 1 in running buffer, 10 mM BCB, and 1 mM BCB as shown in the microchip electropherograms in Fig. 6b. A comparison of peak height shows 1.7- and 1.2-fold increases in signal for the samples in 1 mM BCB and 10 mM BCB, respectively, compared with running buffer. A comparison of the number of theoretical plates shows 1.7- and 1.5-fold increases for the samples in 1 mM BCB and 10 mM BCB, respectively, compared with running buffer. Pressure-driven injection successfully facilitates the μ CE analysis of samples of different ionic strength; with decreasing conductivity, a significant improvement in the number of theoretical plates as well as peak height is obtained. Although stacking is possible with electrokinetic injection, applying voltages to solutions with different conductance values complicates device operation; in contrast, our approach provides direct stacking of sample only in the separation channel.

Comparison with electrokinetic injection

Our pressure-driven injection approach has several advantages. The injection is not biased by analyte mobilities even at very short (<5 s) injection times, the injected plug volume can be controlled through valve spacing, and injection can be performed on solutions over a range of ionic strengths. To highlight some of these benefits, we compared pressure-driven injection to conventional pinched electrokinetic injection [34, 35]. Figure 7 shows microchip electropherograms of FITC-labeled FA, FGGF, and GGYR for 30 s pressure-driven and electrokinetic injections. A comparison of peak height shows 3.5-, 3.1-, and 3.9-fold increases for FA, FGGF, and GGYR, respectively, for pressure-driven compared to electrokinetic injection with the same injection time and separation voltage. The greater peak heights for pressure-based injection can be explained by comparing the sample volumes loaded. The sample volume injected using our method (\sim 300 pL, defined by valve spacing) is a factor of 5 greater than the volume loaded in electrokinetic injection (\sim 60 pL, defined by the intersection volume). On the other hand, the number of theoretical plates for all three peaks was essentially the same for both injection methods. Our results show that pressure-driven injection can improve signal in μ CE compared to pinched injection, while keeping similar separation efficiency.

PTB biomarker separation

Finally, to demonstrate the applicability of these devices for real samples, we separated a mixture of FITC-labeled PTB biomarkers, peptide 1 and ferritin, as shown in Fig. 8. The peptide 1 peak is narrower than the ferritin peak, most likely because peptide 1 has only one amine group while ferritin has multiple amines that can be labeled. The PTB biomarker peaks are resolved but not to baseline; this might be due to

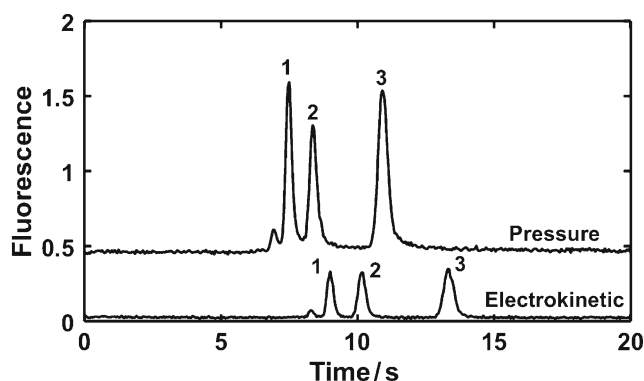


Fig. 7 Comparison of pressure-driven vs. electrokinetic injection. Microchip electropherograms of three peptides, 1 FA, 2 FGGF, and 3 GGYR, each 300 nM, using pressure-driven and electrokinetic injection, with 30 s injection times. Electropherograms are offset vertically. For pressure-driven injection, a 50-ms actuation rate and 200- μ m valve spacing were used

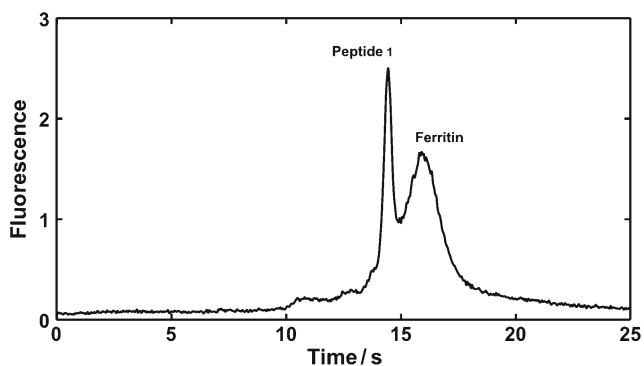


Fig. 8 Microchip electropherogram of FITC-labeled peptide 1 (500 nM) and ferritin (100 nM) using pressure-driven injection with a 50-ms pump actuation rate, 30-s injection time, and 200- μ m valve spacing

the short (1 cm) separation distance in our μ CE device or broadening of the ferritin peak due to stochastic labeling of different numbers of amine groups. Our successful separation and detection of these PTB biomarkers suggest strong potential for future application in more highly integrated systems.

Conclusions

We have developed microfluidic devices with pressure-driven injection for electrophoretic separation and fluorescence detection. The devices have three-layer PDMS construction with a channel fluidic layer, a thin membrane layer, and a control layer with a peristaltic pump and pneumatic valves for sample injection. We studied the effects of the peristaltic pump actuation rate and injection time and chose a 50-ms actuation rate and a 30-s injection time that offered a good combination of speed, peak height, and number of theoretical plates (as much as 500,000 plates/m or more). We evaluated four different valve spacings (100, 200, 300, and 400 μ m) and chose 200 μ m as providing the best peak height. We also studied the effects of stacking and determined that a decrease in the sample conductivity increased the peak height as well as the number of theoretical plates. A comparison was made between pressure-driven and electrokinetic injection for the same injection time and separation voltage; we found that with a comparable number of theoretical plates, the peak height increased significantly for pressure-driven injection. Finally, we showed μ CE analysis of two pre-term birth biomarkers, ferritin and peptide 1, in <1 min using pressure-driven injection.

Key advantages of our approach are the elimination of the mobility bias in injection; control of the volume of injected plug through designed valve spacings; and the ability to inject samples in various solutions, facilitating sample stacking, for example. Our method leads to more than a threefold increase in peak height relative to conventional electrokinetic injection. The use of PDMS to make devices may eventually limit their

applicability and performance. However, we note that we have recently developed alternate materials for microfluidic valves that may address this concern [36, 37].

Currently, we are developing a fully integrated microfluidic device for pre-term birth diagnosis, such that future work will involve the optimization and integration of pressure-driven injection with other sample preparation operations. Notably, although this work is directed at building an integrated device for rapid determination of pre-term birth risk, the general nature of our approach should be broadly applicable for various other biomarkers associated with diseases.

Acknowledgments Funding for this work was provided by the National Institutes of Health under grant R01 EB006124. We thank the Integrated Microfabrication Laboratory at Brigham Young University for device fabrication facilities.

Compliance with ethical standards

Conflict of interest The authors declare that they have no competing interests.

References

1. Culbertson CT, Mickleburgh TG, Stewart-James SA, Sellens KA, Pressnall M (2014) Micro total analysis systems: fundamental advances and biological applications. *Anal Chem* 86:95–118
2. Kovarik ML, Gach PC, Ormoff DM, Wang Y, Balowski J, Farrag L, Allbritton NL (2012) Micro total analysis systems for cell biology and biochemical assays. *Anal Chem* 84:516–540
3. Nge PN, Rogers CI, Woolley AT (2013) Advances in microfluidic materials, functions, integration, and applications. *Chem Rev* 113: 2550–2583
4. Shields CW IV, Reyes CD, López GP (2015) Microfluidic cell sorting: a review of the advances in the separation of cells from bulking to rare cell isolation. *Lab Chip* 15:1230–1249
5. Kantak C, Chang C-P, Wong CC, Mahyuddin A, Choolani M, Rahman A (2014) Lab-on-a-chip technology: impacting non-invasive prenatal diagnostics (NIPD) through miniaturisation. *Lab Chip* 14:841–854
6. Yang R, Pagaduan JV, Yu M, Woolley AT (2015) On chip preconcentration and fluorescence labeling of model proteins by use of monolithic columns: device fabrication, optimization, and automation. *Anal Bioanal Chem* 407:737–747
7. Yang W, Yu M, Sun X, Woolley AT (2010) Microdevices integrating affinity columns and capillary electrophoresis for multibiomarker analysis in human serum. *Lab Chip* 10: 2527–2533
8. Nwankire CE, Venkatanarayanan A, Glennon T, Keyes TE, Forster RJ, Ducrée J (2015) Label-free impedance detection of cancer cells from whole blood on an integrated centrifugal microfluidic platform. *Biosens Bioelectron* 68:382–389
9. Drechsel L, Schulz M, von Stetten F, Moldovan C, Zengerle R, Paust N (2015) Electrochemical pesticide detection with autodip—a portable platform for automation of crude sample analyses. *Lab Chip* 15:704–710
10. Sun Y, Quyen TL, Hung TQ, Chin WH, Wolff A, Bang DD (2015) A lab-on-a-chip system with integrated sample preparation and

- loop-mediated isothermal amplification for rapid and quantitative detection of salmonella spp. in food samples. *Lab Chip* 15:1898–1904
11. Castro ER, Manz A (2015) Present state of microchip electrophoresis: state of the art and routine applications. *J Chromatogr A* 1382:66–85
 12. Nuchtavorn N, Suntornsuk W, Lunte SM, Suntornsuk L (2015) Recent applications of microchip electrophoresis to biomedical analysis. *J Pharm Biomed Anal* 113:72–96
 13. Saylor RA, Lunte SM (2015) A review of microdialysis coupled to microchip electrophoresis for monitoring biological events. *J Chromatogr A* 1382:48–64
 14. Karlinsey JM (2012) Sample introduction techniques for microchip electrophoresis: a review. *Anal Chim Acta* 725:1–13
 15. Pagaduan JV, Ramsden M, O'Neill K, Woolley AT (2015) Microchip immunoaffinity electrophoresis of antibody–thymidine kinase 1 complex. *Electrophoresis* 36:813–817
 16. Zhuang B, Gan W, Wang S, Han J, Xiang G, Li C-X, Sun J, Liu P (2015) Fully automated sample preparation microsystem for genetic testing of hereditary hearing loss using two-color multiplex allele-specific PCR. *Anal Chem* 87:1202–1209
 17. Tsai C-H, Yang R-J, Tai C-H, Fu L-M (2005) Numerical simulation of electrokinetic injection techniques in capillary electrophoresis microchips. *Electrophoresis* 26:674–686
 18. Alarie JP, Jacobson SC, Ramsey JM (2001) Electrophoretic injection bias in a microchip valving scheme. *Electrophoresis* 22:312–317
 19. Dossi N, Toniolo R, Susmel S, Pizzariello A, Bontempelli G (2010) A simple approach to the hydrodynamic injection in microchip electrophoresis with electrochemical detection. *Electrophoresis* 31:2541–2547
 20. Chen C-C, Yen S-F, Makamba H, Li C-W, Tsai M-L, Chen S-H (2007) Semihydrodynamic injection for high salt stacking and sweeping on microchip electrophoresis and its application for the analysis of estrogen and estrogen binding. *Anal Chem* 79:195–201
 21. Li MW, Martin RS (2008) Microchip-based integration of cell immobilization, electrophoresis, post-column derivatization, and fluorescence detection for monitoring the release of dopamine from PC 12 cells. *Analyst* 133:1358–1366
 22. Mecker LC, Martin RS (2008) Integration of microdialysis sampling and microchip electrophoresis with electrochemical detection. *Anal Chem* 80:9257–9264
 23. Saito RM, Coltro WKT, de Jesus DP (2012) Instrumentation design for hydrodynamic sample injection in microchip electrophoresis: a review. *Electrophoresis* 33:2614–2623
 24. Bai X, Lee HJ, Rossier JS, Reymond F, Schafer H, Wossner M, Girault HH (2002) Pressure pinched injection of nanolitre volumes in planar micro-analytical devices. *Lab Chip* 2:45–49
 25. Lin CC, Chen CC, Lin CE, Chen SH (2004) Microchip electrophoresis with hydrodynamic injection and waste-removing function for quantitative analysis. *J Chromatogr A* 1051:69–74
 26. Bowen AL, Martin RS (2010) Integration of on-chip peristaltic pumps and injection valves with microchip electrophoresis and electrochemical detection. *Electrophoresis* 31:2534–2540
 27. Reich ES (2012) Pre-term births on the rise. *Nature* 485:20
 28. Hofman PL, Regan F, Jackson WE, Jefferies C, Knight DB, Robinson EM, Cutfield WS (2004) Premature birth and later insulin resistance. *N Engl J Med* 351:2179–2186
 29. Allin M, Matsumoto H, Santhouse AM, Nosarti C, AlAsady MHS, Stewart AL, Rifkin L, Murray RM (2001) Cognitive and motor function and the size of the cerebellum in adolescents born very pre-term. *Brain* 124:60–66
 30. Goldenberg RL, Goepfert AR, Ramsey PS (2005) Biochemical markers for the prediction of preterm birth. *Am J Obstet Gyn* 192:S36–S46
 31. Esplin MS, Merrell K, Goldenberg R, Lai Y, Iams JD, Mercer B, Spong CY, Miodovnik M, Simhan HN, van Dorsten P, Dombrowski M (2011) Proteomic identification of serum peptides predicting subsequent spontaneous preterm birth. *Am J Obstet Gyn* 204:391.e1–391.e8
 32. Graves SW, Esplin MS (2011) Validation of predictive preterm birth biomarkers obtained by maternal serum proteomics. *Am J Obstet Gyn* 204:S46
 33. Esplin MS (2012) Proteomic identification of serum peptides predicting subsequent spontaneous preterm birth reply. *Am J Obstet Gyn* 206:E3–E4
 34. Jacobson SC, Hergenroder R, Koutny LB, Warmack RJ, Ramsey JM (1994) Effects of injection schemes and column geometry on the performance of microchip electrophoresis devices. *Anal Chem* 66:1107–1113
 35. Kelly RT, Woolley AT (2003) Thermal bonding of polymeric capillary electrophoresis microdevices in water. *Anal Chem* 75:1941–1945
 36. Rogers CI, Oxborrow JB, Anderson RR, Tsai L-F, Nordin GP, Woolley AT (2014) Microfluidic valves made from polymerized polyethylene glycol diacrylate. *Sensors Actuators B Chem* 191:438–444
 37. Rogers CI, Qaderi K, Woolley AT, Nordin GP (2015) 3D printed microfluidic devices with integrated valves. *Biomicrofluidics* 9:016501